Computer Modeling in Engineering & Sciences CMES, vol.122, no.3, pp.889-906, 2020

Impact Dynamics of a Dragonfly Wing

Lihua Wang[1, *], Wenjing Ye[1] and Yueting Zhou[1]

Abstract: The lift force was reported not to be high enough to support the dragonfly's weight during flight in some conventional investigations, and higher lift force is required for its takeoff. In this study, by employing a thin plate model, impact effect is investigated for the wing deformation in dragonfly flapping during takeoff. The static displacement is formulated to compare with the dynamical displacement caused by impact. The governing equation of motion for the impact dynamics of a dragonfly wing is derived based on Newton's second law. Separation of variables technique and assumed modes method are introduced to solve the resulting equations. Further, lift force is presented for the cases of considering and without considering the impact on the wing flapping which indicates that the impact has prominent effects for the dragonfly's aerodynamic performance. Numerical simulations demonstrate that considering the impact effect on the wing flapping can increase the wing deformation, which results in the rise of the lift force. The enhanced lift force is of critical importance for the dragonfly's takeoff.

Keywords: Impact dynamics, wing deformation, thin plate model, lift force.

1 Introduction

Dragonfly has excellent flying abilities because it can produce and control aerodynamic forces through a large variety of wingbeat kinematics. To explain the force production during dragonfly's flight, in the early stage, Weis-Fogh [Weis-Fogh (1973)] proposed two mechanisms of lift generation referring to "clap and fling" and "flip" based on a quasi-steady state model, in which the steady-state forces were assumed to be produced by the wing at each instantaneous position. Later on, Azuma et al. [Azuma, Azuma, Watanabe et al. (1985)] filmed the steady slow climbing flight of a dragonfly and explored the mechanical characteristics of its beating wings. Their results showed that the dragonfly performed low speed flight with ordinary airfoil characteristics, instead of adopting an abnormally large lift coefficient. Furthermore, Azuma et al. [Azuma and Watanabe (1988)] examined a dragonfly in free flight and found that the dragonfly could make steady trimmed flight at various flight speeds, from hovering to top speed, without using any novel unsteady aerodynamic force generated by a separated flow over the wings.

Although the early investigations indicated that, based on the observations of wing kinematics, steady analysis could explain the lift generation for dragonfly's flight, Norberg [Norberg (1975)] computed the average minimum force coefficients using steady-state

[1] School of Aerospace Engineering and Applied Mechanics, Tongji University, Shanghai, China.

[*] Corresponding Author: Lihua Wang. Email: lhwang@tongji.edu.cn.

Received: 02 November 2019; Accepted: 25 December 2019.

aerodynamics and at most only 40% of the upward force needed during hovering could be obtained. This concluded that the steady-state aerodynamics was incapable of explaining how the dragonfly supported its weight during hovering. Moreover, the required lift coefficients based on the quasi-steady state theory were reported to be higher than those actually measured [Ellington (1984a)]. Lehmann [Lehmann (2004)] pointed out that compared to the predictions from conventional steady-state aerodynamic theory, these unsteady aerodynamic mechanisms might account for the majority of total lift produced by a flying insect. On the basis of qualitative free- and tethered-flight flow visualization, Thomas et al. [Thomas, Taylor, Srygley et al. (2004)] testified the dragonfly's flight using unsteady aerodynamic mechanisms to generate high-lift and leading edge vortices. Besides, an alternative lift-generating mechanism was proposed by employing the flow field during a complete cycle of the idealized wing motion performed in water and unsteady inviscid flow theory, based on which a plausible balance of horizontal forces and more than sufficient lift could be obtained [Savage (1979)].

Quasi-steady and unsteady dynamics are often studied in the hovering motion along a horizontal stroke plane where the aerodynamic drag makes no contribution to the vertical force. While in the inclined stroke planes, the drag in the down- and upstrokes does not cancel each other, which may need to be considered in the computation of dragonfly's lift generation. Sun et al. [Sun and Lan (2004)] analyzed the aerodynamic force generation and mechanical power requirements of a dragonfly in hovering flight. They concluded that during the hovering with a large stroke plane angle, the dragonfly used drag as a major source for its weight supporting force and the vertical force coefficient of a wing was twice as large as the quasi-steady value. Wang [Wang (2004)] presented that a dragonfly used drag to support about three quarters of its weight during hovering by calculating an idealized dragonfly wing motion. Wakeling et al. [Wakeling and Ellington (1997)] photographed the free gliding flight of the dragonfly and presented that the maximum lift coefficient recorded from these glides was 0.93. However, higher lift coefficient could be detected when considering the drag forces since the linear dependence of drag on velocity should be included to predict the parasite drag on dragonflies at non-zero body angles.

Some other researchers studied the influences from the characterized details of the dragonfly wings. Combes et al. [Combes and Daniel (2003)] proposed that the aerodynamic force production was quite sensitive to subtle changes in the shape of insect wings. The highly corrugated dragonfly wings introduce a lightweight structure and produce at times higher lift and moderate drag compared to the profiled airfoil [Obata, Shinohara, Akimoto et al. (2014); Uppu, Manisha, Devi et al. (2018); Dwivedi and Bhargava (2019); Ho, New and Matare (2017)]. Zhao et al. [Zhao, Yin and Zhong (2010)] discovered the micro and nano structures and morphologies on the surfaces of the veins of dragonfly wings, in which spikes and ripple wave morphologies might contribute remarkably to the lift (thrust) mechanisms of dragonflies. Wang et al. [Wang and Zhong (2014, 2015, 2018)] presented that blood circulation in the veins of the dragonfly wings had a stabilization effect on the system, which supported the dragonfly could achieve active control by regulating the distribution of the blood in a dynamic process [Zhao, Yin and Zhong (2013)]. Hou et al. [Hou, Yin, Zhong et al. (2015a, b)] proposed a new torsion control mechanism generated by blood circulation and investigated the influences on the dragonfly wing's vibration characteristics caused by the blood in veins. Besides,

interactions between the fore- and hindwings were also investigated for the lift of dragonfly wings. The interactions were first reported to be detrimental to the vertical force generation [Sun and Lan (2004)]. However, Usherwood et al. [Usherwood and Lehmann (2008)] subsequently proposed that, despite presenting no advantage in terms of lift, flying with two pairs of wings could be highly effective at improving aerodynamic efficiency and had the ability to control aerodynamic performance by modulating the phase lag between forewings and hindwings [Wang and Russell (2007); Maybury and Lehmann (2004); Salami, Ward, Montazer et al. (2019)].

In most previous studies, the dragonfly wings were usually modeled as stiff, flat plates. However, more and more investigations presented that some bending and twist in flight had large aerodynamic effects [Alexander (2000); Zhu, Zhou, Wang et al. (2014); Shumway and Laurence (2019)] and the lift could be increased with a deformation [Du and Sun (2008)]. Most of the explorations examined the wing flexibility in aerodynamic analysis by solving the Navier-Stokes equations. Nevertheless, accumulated evidences from both experimental and theoretical studies proved that inertial deformation overshadowed aeroelastic deformation in wing functioning [Daniel and Combes (2002); Bergou, Xu and Wang (2007); Hedrick, Combes and Miller (2014)]. On the other hand, higher lift force is required for takeoff than hovering [Alexander (1984)] and clap-and-fling is the most popular lift-generating mechanism in takeoff [Weis-Fogh (1973)]. Most of the conventional work detailedly studied the lift-generating in hovering after takeoff, while the required high lift force for dragonfly's takeoff is still lack of investigation. Therefore, in this work, impact dynamics is first studied for the dragonfly's wing flapping during takeoff. An impact model is set up and the governing equations of motion for the impulse loading and free vibration are formulated, where the rigid body rotation of the wing does not considered. Displacements and resulting lift forces considering and without considering the impact effect are simulated for comparison.

2 Static displacement of the cantilever plate

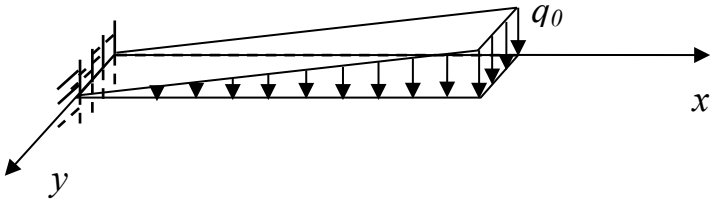

Figure 1: Model of a dragonfly wing

As shown in Fig. 1, wing flapping is modeled as a fixed axis rotation around y-axis during the dragonfly's takeoff, and the wing is modeled by a cantilever thin plate. Based on the measurement of Takahashi et al. [Takahashi, Sato, Matsumoto et al. (2014)], the equivalent distribution load acting on the plate during the takeoff can be assumed as

$$q(x,y)=q_0\frac{x}{l} \tag{1}$$

where $q(x,y)$ is the load per unit area, l is the length of the plate and q_0 is a constant. The equilibrium equation for a thin plate can be expressed as

$$\frac{\partial^4 w_s}{\partial x^4}+2\frac{\partial^2 w_s}{\partial x^2\partial y^2}+\frac{\partial^4 w_s}{\partial y^4}=\frac{q(x,y)}{D} \tag{2}$$

where w_s is the static transverse displacement, $D=Eh^3/12(1-\nu^2)$ is the flexural rigidity of the plate in which E is the Young's modulus, ν is the Poisson's ratio and h is the thickness of the plate. The boundary conditions of the cantilever plate are

$$w_s\big|_{x=0}=0\,,\quad \left.\frac{\partial w_s}{\partial x}\right|_{x=0}=0 \tag{3}$$

$$\begin{aligned} M_x\big|_{x=l}&=-D\left(\frac{\partial^2 w_s}{\partial x^2}+\nu\frac{\partial^2 w_s}{\partial y^2}\right)\Bigg|_{x=l}=0\\ V_x\big|_{x=l}&=-D\left(\frac{\partial^3 w_s}{\partial x^3}+(2-\nu)\frac{\partial^3 w_s}{\partial x\partial y^2}\right)\Bigg|_{x=l}=0 \end{aligned} \tag{4}$$

$$\begin{aligned} M_y\big|_{y=0}&=-D\left(\frac{\partial^2 w_s}{\partial y^2}+\nu\frac{\partial^2 w_s}{\partial x^2}\right)\Bigg|_{y=0}=0\\ V_y\big|_{y=0}&=-D\left(\frac{\partial^3 w_s}{\partial y^3}+(2-\nu)\frac{\partial^3 w_s}{\partial x^2\partial y}\right)\Bigg|_{y=0}=0 \end{aligned} \tag{5}$$

$$\begin{aligned} M_y\big|_{y=b}&=-D\left(\frac{\partial^2 w_s}{\partial y^2}+\nu\frac{\partial^2 w_s}{\partial x^2}\right)\Bigg|_{y=b}=0\\ V_y\big|_{y=b}&=-D\left(\frac{\partial^3 w_s}{\partial y^3}+(2-\nu)\frac{\partial^3 w_s}{\partial x^2\partial y}\right)\Bigg|_{y=b}=0 \end{aligned} \tag{6}$$

in which b is the width of the plate. The two free corners $(l,0)$ and (l,b) require

$$2D(1-\nu)\frac{\partial^2 w_s}{\partial x\partial y}=0 \tag{7}$$

Solution of Eq. (2) can be expressed as [Chang (1980)]

$$
\begin{aligned}
w_s(x,y) &= \frac{1-\nu}{2}\sum_{j=1,3..}\frac{c_j}{\operatorname{sh}\alpha_j}\left\{\left(\frac{2}{1-\nu}+c_j\coth\alpha_j\right)\operatorname{sh}\frac{j\pi x}{b}-\frac{j\pi x}{b}\operatorname{ch}\frac{j\pi x}{b}\right\}\sin\frac{j\pi y}{b}\\
&+\frac{1-\nu}{2}\sum_{i=1,2..}b_i\left\{\begin{array}{l}\dfrac{\operatorname{ch}\beta_i-1}{\operatorname{sh}\beta_i}\left[\left(\dfrac{\beta_i}{\operatorname{sh}\beta_i}-\dfrac{2}{1-\mu}\right)\operatorname{sh}\dfrac{i\pi y}{l}+\dfrac{i\pi y}{l}\operatorname{ch}\dfrac{i\pi y}{l}\right]+\\ \dfrac{2}{1-\mu}\operatorname{ch}\dfrac{i\pi y}{l}-\dfrac{i\pi y}{l}\operatorname{sh}\dfrac{i\pi y}{l}\end{array}\right\}\sin\frac{i\pi x}{l}\\
&+\frac{b^2}{2D\pi^2}\sum_{j=1,3..}\frac{r_j}{j^2}\left\{-\frac{\alpha_j}{\operatorname{sh}^2\alpha_j}\operatorname{sh}\frac{j\pi x}{b}-\frac{j\pi x}{b}\operatorname{sh}\frac{j\pi x}{b}+\coth\alpha_j\frac{j\pi x}{b}\operatorname{ch}\frac{j\pi x}{b}\right\}\sin\frac{j\pi y}{b}\\
&+\frac{4q_0b^4x}{D\pi^5l}\sum_{j=1,3...}\frac{1}{j^5}\left\{1-\operatorname{ch}\frac{j\pi y}{b}+\frac{1}{2}\frac{j\pi y}{b}\operatorname{sh}\frac{j\pi y}{b}\right.\\
&\left.-\frac{\operatorname{ch}\alpha_j-1}{2\operatorname{sh}\alpha_j}\left[\frac{j\pi y}{b}\operatorname{ch}\frac{j\pi y}{b}-2\left(1-\frac{\alpha_j}{2\operatorname{sh}\alpha_j}\right)\operatorname{sh}\frac{j\pi y}{b}\right]\right\}\sin\frac{j\pi x}{b}+\eta x
\end{aligned}
\tag{8}
$$

where

$$
\alpha_j=\frac{j\pi L}{b},\quad \beta_i=\frac{i\pi b}{L} \tag{9}
$$

and the coefficients c_j, b_i, r_j, η can be obtained from substituting the solution (8) into the following boundary conditions equations

$$
\begin{aligned}
&\left.\frac{\partial w_s}{\partial x}\right|_{x=0}=0,\\
&V_x\big|_{x=l}=-D\left(\frac{\partial^3 w_s}{\partial x^3}+(2-\nu)\frac{\partial^3 w_s}{\partial x\partial y^2}\right)\Bigg|_{x=l}=0,\\
&V_y\big|_{y=b}=-D\left(\frac{\partial^3 w_s}{\partial y^3}+(2-\nu)\frac{\partial^3 w_s}{\partial x^2\partial y}\right)\Bigg|_{y=b}=0,\\
&\left(2D(1-\nu)\frac{\partial^2 w_s}{\partial x\partial y}\right)_{\substack{x=l\\y=0}}=0
\end{aligned}
\tag{10}
$$

The resulting equations for obtaining the coefficients can be found in the appendix A.

3 Impact dynamics of the cantilever plate

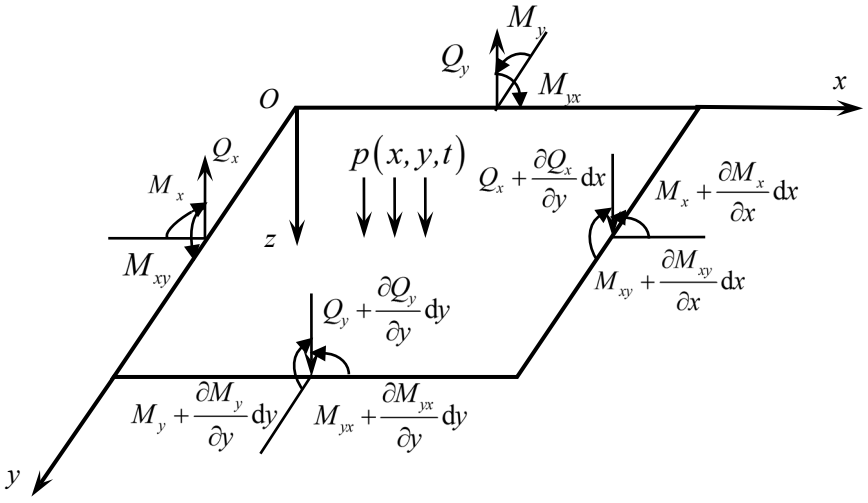

Figure 2: A thin plate subjected to transverse distributed load

Consider a rectangular thin plate of uniform thickness h as shown in Fig. 2. The $xoy(z=0)$ plane coincides with the mid-plane of the thin plate. Based on Kirchhoff thin plate theory, the governing equation of a thin plate subjected to dynamical load can be formulated as [Chu, Wang, Zhong et al. (2014)]

$$\frac{\partial^4 w}{\partial x^4}+2\frac{\partial^4 w}{\partial x^2\partial y^2}+\frac{\partial^4 w}{\partial y^4}+\frac{\rho h}{D}\frac{\partial^2 w}{\partial t^2}=\frac{p(x,y,t)}{D} \tag{11}$$

where w is the tranverse displacement of the thin plate, ρ is the density of the plate and $p(x,y,t)$ is the dynamical load per unit area, which represents the action force from the dragonfly's wing flapping. When considering the rectangular impulsive load, for $t\le t_0$, $p(x,y,t)=p_0\frac{x}{l}$, and for $t>t_0$, $p(x,y,t)=0$. Here t_0 is the action time of impulsive load.

Based on separation of variables technique [Wang, Hu, Zhong et al. (2009, 2010)], the solution of Eq. (11) takes the form

$$w(x,y,t)=\sum_{i=1}^{N}\phi_j(x,y)d_j(t) \tag{12}$$

where $\phi_j(x,y)$ is the approximation function, and $d_j(t)$ is the node coefficient. Substituting Eq. (12) into Eq. (11), multiplying the equation by $\phi_i(x,y)$ and integrating it from $x=0$ to l and $y=0$ to b, we obtain the discretized equation of motion

$$\mathbf{M}\ddot{\mathbf{d}}(t)+\mathbf{K}\mathbf{d}(t)=\mathbf{f}(t) \tag{13}$$

where

$$M_{ij} = \rho h \int_0^b \int_0^l \phi_i \, \phi_j \, \mathrm{d}x \, \mathrm{d}y \tag{14}$$

$$K_{ij} = D \int_0^b \int_0^l \phi_i \left(\frac{\partial \phi_j^4}{\partial x} + 2 \frac{\partial \phi_j^2}{\partial x} \frac{\partial \phi_j^2}{\partial y} + \frac{\partial \phi_j^4}{\partial y} \right) \mathrm{d}x \, \mathrm{d}y \tag{15}$$

$$f_i = \int_0^b \int_0^l \left(p + \rho h g \right) \phi_i \, \mathrm{d}x \, \mathrm{d}y \tag{16}$$

The approximation function can be expressed as

$$\phi_j \left(x, y \right) = X_m \left(x \right) Y_n \left(y \right) \tag{17}$$

where $m = 1, 2 \cdots N_l$, $n = 1, 2 \cdots N_b$, and $j = \left(m - 1 \right) N_b + n$. Thus, the number of terms assumed for a trial function can be denoted by $N = N_l \times N_b$, where N_l and N_b are the numbers of terms in the x and y directions, respectively. The trial functions are

$$\begin{aligned} &X_m \left(x \right) = \left[\mathrm{ch}\left(\alpha_m x \right) - \cos\left(\alpha_m x \right) \right] - C_m \left[\mathrm{sh}\left(\alpha_m x \right) - \sin\left(\alpha_m x \right) \right] \quad \left(m = 1, 2 \cdots \right); \\ &C_m = \frac{\mathrm{ch}\left(\alpha_m l \right) + \cos\left(\alpha_m l \right)}{\mathrm{sh}\left(\alpha_m l \right) + \sin\left(\alpha_m l \right)}; \\ &\alpha_1 = \frac{1.87510}{l}, \alpha_2 = \frac{4.69409}{l}, \alpha_3 = \frac{7.85476}{l}, \alpha_m = \frac{\left(2m - 1 \right) \pi}{2l}, \left(m = 4, 5 \cdots \right). \end{aligned} \tag{18}$$

and

$$\begin{aligned} &Y_1 \left(y \right) = 1 \quad ; \quad Y_2 \left(y \right) = \sqrt{3} \left(1 - \frac{2y}{b} \right); \\ &Y_n \left(y \right) = \left[\mathrm{ch}\left(\beta_n y \right) + \cos\left(\beta_n y \right) \right] - C_n \left[\mathrm{sh}\left(\beta_n y \right) + \sin\left(\beta_n y \right) \right] \quad \left(n = 3, 4 \cdots \right); \\ &C_n = \frac{\mathrm{ch}\left(\beta_n b \right) - \cos\left(\beta_n b \right)}{\mathrm{sh}\left(\beta_n b \right) - \sin\left(\beta_n b \right)}; \\ &\beta_3 = \frac{4.73004}{b}, \beta_4 = \frac{7.85320}{b}, \beta_n = \frac{\left(2n - 3 \right) \pi}{2b}, \left(n = 5, 6 \cdots \right). \end{aligned} \tag{19}$$

The initial conditions $d_j \left(0 \right), \dot{d}_j \left(0 \right)$ can be obtained as follows

$$d_j \left(0 \right) = \frac{\int_0^b \int_0^l w\left(x, y, 0 \right) \phi_j \left(x, y \right) \mathrm{d}x \, \mathrm{d}y}{\int_0^b \int_0^l \phi_j^2 \left(x, y \right) \mathrm{d}x \, \mathrm{d}y} \tag{20}$$

$$\dot{d}_j \left(0 \right) = \frac{\int_0^b \int_0^l \dot{w}\left(x, y, 0 \right) \phi_j \left(x, y \right) \mathrm{d}x \, \mathrm{d}y}{\int_0^b \int_0^l \phi_j^2 \left(x, y \right) \mathrm{d}x \, \mathrm{d}y} \tag{21}$$

When $t \le t_0$, the initial conditions are

$$w(x,y,0)=w_l\left(\frac{x^5}{l}-10lx^3+20l^2x^2\right),\quad \dot{w}(x,y,0)=v_l x \tag{22}$$

When $t>t_0$, the initial conditions are

$$w(x,y,t_1)=w(t_1),\quad \dot{w}(x,y,t_1)=\dot{w}(t_1) \tag{23}$$

where w_l and v_l are generic constants and $t_1=t-t_0$.

4 Lift force for the plate

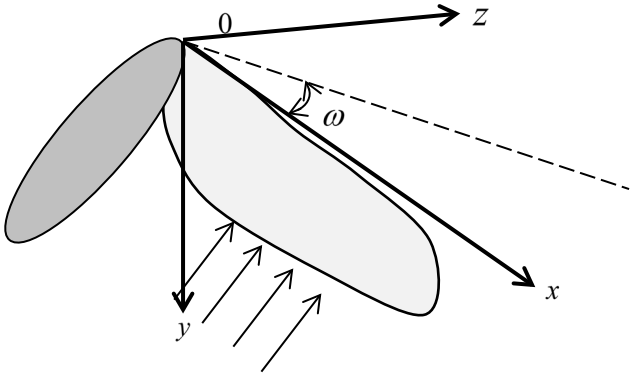

Figure 3: Schematic for the flapping of a wing model around a fixed axis

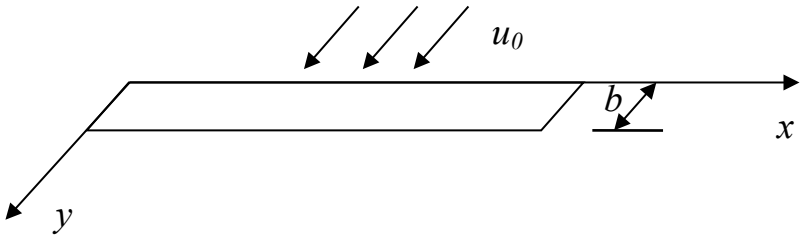

Figure 4: Model of wing flapping

Figure 5: Schematic of wing model and incoming flow

For studying the lift force of the wing, the flapping wing is also modeled by a thin plate as shown in Figs. 3 and 4, and a simplified aerodynamic model is used for numerical evaluation [Tang, Dowell and Hall (1999); Dardel and Bakhtiari-Nejad (2010); Dimitriadis, Giannelis and Vio (2018)]. The verification of this simplified model compared to the

experimental data was presented in Bao [Bao (2007)]. The fixed axis and the incoming flow are along oy direction. As shown in Fig. 5, u_0 is the velocity of the incoming flow, v is the flapping velocity, u is the relative velocity of the fluid, and θ is the angle of attack. Based on the Kutta-Jowkowski theorem [Anderson (1989)], the lift for a model section can be expressed as

$$\mathrm{d}L = \rho_0 u \Gamma \mathrm{d}x = \pi \rho_0 b u^2 \sin\theta \mathrm{d}x \tag{24}$$

where ρ_0 is the fluid density, b is the chord length of the thin plate, and Γ is the circulation. The component perpendicular to the direction of the flow is

$$\mathrm{d}L_1 = \pi \rho_0 b u^2 \sin\theta \mathrm{d}x \cdot \cos\theta \tag{25}$$

where $\tan\theta = v/u_0$, $u^2 = v^2 + u_0^2$. Substituting these two equations into Eq. (25) renders

$$\mathrm{d}L_1 = \pi \rho_0 b v u_0 \mathrm{d}x \tag{26}$$

The added mass effect originated from the nonuniform motion can be written as [Bao (2007)]

$$\mathrm{d}L_2 = \frac{\pi}{4} \rho_0 b^2 \dot{v} \mathrm{d}x \tag{27}$$

The average velocity is introduced for comparison where $v_s = \dfrac{w_s}{\Delta t}$, $v = \dfrac{\max\left(w(x,y,t)\right)}{\Delta t} = \dfrac{w_m(x,y)}{\Delta t}$ and $w_m(x,y)$ is the maximum of $w(x,y,t)$. Then we have

$$L_s = \int_0^l \mathrm{d}L_1 + \int_0^l \mathrm{d}L_2 = \int_0^l \pi \rho_0 b u_0 \frac{w_s}{\Delta t} \mathrm{d}x + \int_0^l \frac{\pi}{4} \rho_0 b^2 \frac{\mathrm{d}}{\mathrm{d}t}\left(\frac{w_s}{\Delta t}\right) \mathrm{d}x \tag{28}$$

$$L_m = \int_0^l \mathrm{d}L_1 + \int_0^l \mathrm{d}L_2 = \int_0^l \pi \rho_0 b u_0 \frac{w_m}{\Delta t} \mathrm{d}x + \int_0^l \frac{\pi}{4} \rho_0 b^2 \frac{\mathrm{d}}{\mathrm{d}t}\left(\frac{w_m}{\Delta t}\right) \mathrm{d}x \tag{29}$$

Eqs. (28) and (29) give the ratio of the lift forces

$$\xi = \frac{L_m}{L_s} = \frac{\int_0^l \pi \rho_0 b u_0 \dfrac{w_m}{\Delta t} \mathrm{d}x + \int_0^l \dfrac{\pi}{4} \rho_0 b^2 \dfrac{\mathrm{d}}{\mathrm{d}t}\left(\dfrac{w_m}{\Delta t}\right) \mathrm{d}x}{\int_0^l \pi \rho_0 b u_0 \dfrac{w_s}{\Delta t} \mathrm{d}x + \int_0^l \dfrac{\pi}{4} \rho_0 b^2 \dfrac{\mathrm{d}}{\mathrm{d}t}\left(\dfrac{w_s}{\Delta t}\right) \mathrm{d}x} = \frac{4u_0 \int_0^l w_m \mathrm{d}x + b \int_0^l \dot{w}_m \mathrm{d}x}{4u_0 \int_0^l w_s \mathrm{d}x + b \int_0^l \dot{w}_s \mathrm{d}x} \tag{30}$$

where L_s is the lift force without considering the impact effect and L_m is the maximum lift force considering the impact effect. For the wing flapping considering impact influence, we have $v = \dfrac{\partial w(x,y,t)}{\partial t}$ and

$$L = \int_0^l \mathrm{d}L_1 + \int_0^l \mathrm{d}L_2 = \pi \rho_0 b u_0 \int_0^l \frac{\partial w}{\partial t} \mathrm{d}x + \frac{\pi}{4} \rho_0 b^2 \int_0^l \frac{\partial^2 w}{\partial t^2} \mathrm{d}x \tag{31}$$

5 Numerical simulations

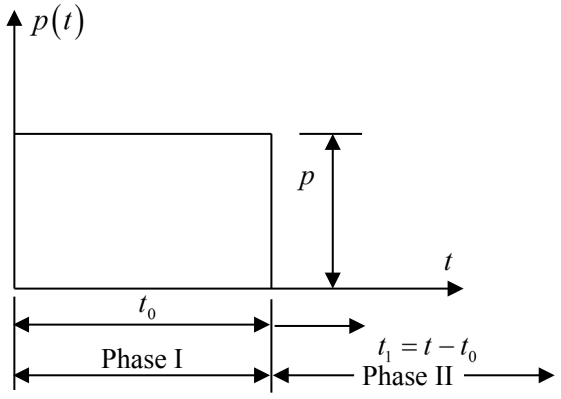

Figure 6: Rectangular impulse

Consider a rectangular thin plate subjected to a rectangular impulsive load as shown in Fig. 6. Span length and chord length of the plate are $l=0.030$ m and $b=0.009$ m, respectively. Thickness of the plate is $h=5\times10^{-4}$ m. Density of the plate is $\rho=1.2\times10^{3}$ kg/m^3. Young's modulus is $E=7.8$ Gpa and Poisson's ratio is $\nu=0.3$ [Ellington (1984b)]. The density of air is $\rho_0=1.29$ kg/m^3. For comparing the dynamical displacement and static displacement, we set $p_0=q_0$. The initial displacement is w_l=0.

The response to the rectangular impulsive load can be divided into two phase: the first phase corresponding to the forced vibration phase in the interval during which the load acts, and the second phase corresponding to the free-vibration which follows. During Phase I ($t\le t_0$), the system is subjected to the rectangular impulse load as shown in Fig. 6 where $p(x,y,t)=p_0\dfrac{x}{l}$. During Phase II ($t>t_0$), the free vibration occurs depending on the displacement $w(t_0)$ and velocity $\dot{w}(t_0)$ existing at the end of Phase I. Under different impulsive loads, the maximum dynamical displacements and static displacements, tip displacements and lift forces for vibrational plate are displayed in Figs 7-9, respectively. These demonstrate that maximum dynamical displacements are bigger than the static displacements, and when load increases, the dynamical displacement increases which leads to the rise of the lift force. Under different loads, the ratios between lift forces considering and without considering the impact are shown in Tab. 1. These indicate that the ratio decreases with the increase of the load. Under different initial velocities, displacements shown in Figs 10 and 11 reveal that higher initial velocity results in higher vibration response and bigger lift force can be observed as shown in Fig. 12. The ratios of lift forces are further exhibited in Tab. 2. When $t_0\ge0.001273$ s=$T_0/2$=$0.3159T$ in which T_0 is the period of the lift force and T is the period of the plate vibration, the peak value of the lift force corresponding to a given impulsive load $p_0=5$ and initial condition $v_l=0.02$ can be obtained. When $t_0\le0.3159T$, the maximum dynamical displacements, tip

displacements and lift forces for the free vibration of the plate are presented in Figs. 13-15 to describe the free vibration after the impulse, respectively. When the time of impulse t_0 increases ($t_0 \le 0.3159T$), the maximum dynamical displacements and lift forces also increase. Since T is quite small for this system, generally, the impulsive loading time can exceed $0.3159T$ and maximum lift force can be achieved. Therefore, when considering the impact effect bigger maximum dynamical displacement and higher lift force can be obtained compared to the case without considering the impact.

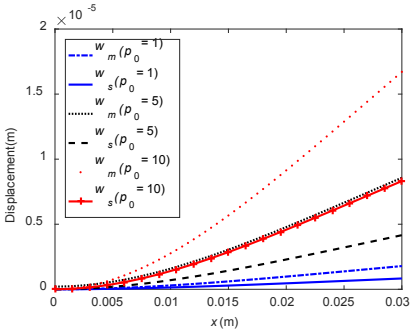

Figure 7: Comparisons of maximum dynamical displacement and static displacement under different loads when $v_l = 0.02$

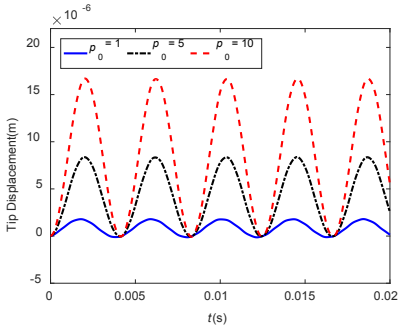

Figure 8: Tip displacements for vibrational plate under different loads when $v_l = 0.02$

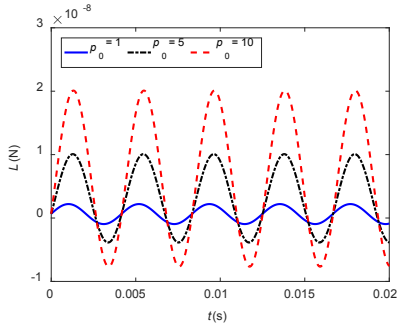

Figure 9: Lift forces for vibrational plate under different loads when $v_l = 0.02$

Table 1: Ratio of lift forces under different loads

$v_l = 0.02$		
$p_0 = 1$	$p_0 = 5$	$p_0 = 10$
$\xi = 4.4935$	$\xi = 4.0911$	$\xi = 4.0776$

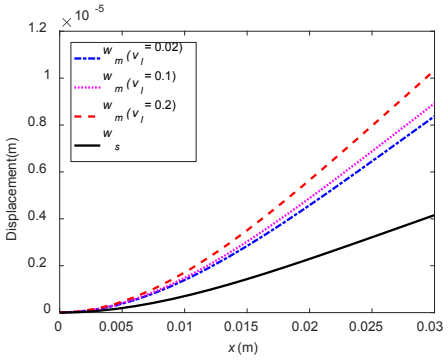

Figure 10: Comparisons of maximum dynamical displacement and static displacement under different initial velocities when $p_0 = 5$

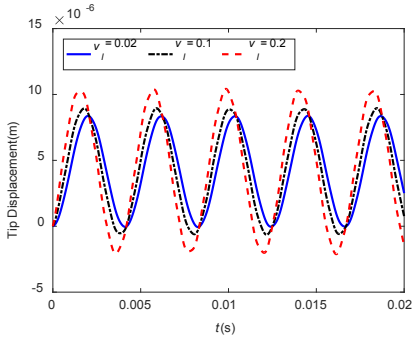

Figure 11: Tip displacements for vibrational plate under different initial velocities when $p_0 = 5$

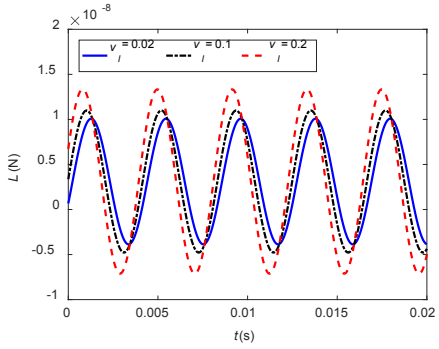

Figure 12: Lift forces for vibrational plate under different initial velocities when $p_0 = 5$

Table 2: Ratio of lift forces under different initial velocities

$p_0 = 5$		
$v_l = 0.02$	$v_l = 0.1$	$v_l = 0.2$
$\xi = 4.0911$	$\xi = 4.4934$	$\xi = 5.5252$

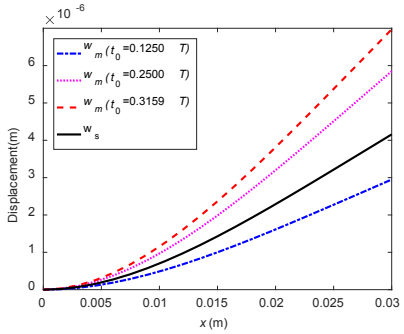

Figure 13: Comparisons of maximum dynamical displacement and static displacement under different time of impulse loading when $p_0 = 5$, $v_l = 0.02$

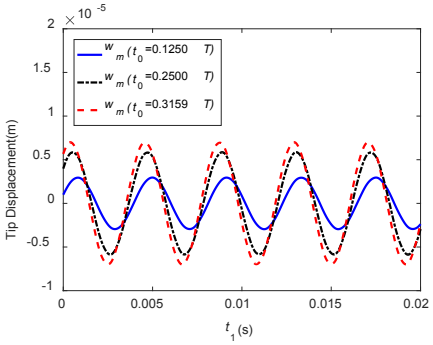

Figure 14: Tip displacements for vibrational plate under different time of impulse loading when $p_0 = 5$, $v_l = 0.02$

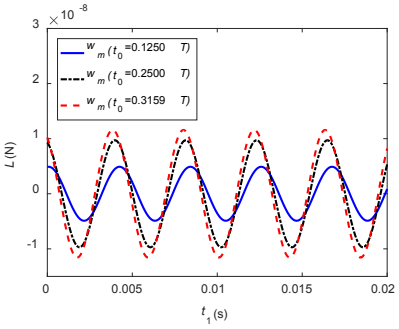

Figure 15: Lift forces for vibrational plate under different time of impulse loading when $p_0 = 5$, $v_l = 0.02$

6 Conclusion

In this work, impact effect is studied to evaluate the dynamical response for the dragonfly's wing flapping during takeoff. The governing equations of motion for the impulse forced vibration and free vibration are formulated. Lift forces are computed based on the dynamical displacements. When considering the impact effect during the dragonfly's wing clapping, the response has two phase, in which phase I is corresponding to the forced vibration raised by the impulse, and phase II is corresponding to the free vibration raised by the initial vibration existing at the end of Phase I. When $t_0 \geq T_0/2$ (T_0 is the period of the lift force), the system can achieve maximum lift force, which is several times higher than that obtained from the static deformation. When $t_0 < T_0/2$, higher lift force can be received with the increase of the impulsive loading time. In general, we may attain maximum lift force since the period of the system T is quite small and $T_0 < T$. Compared to the static displacement and the resulting lift force in the conventional model, it can be concluded that the model considering the impact effect in dragonfly's wing clapping during takeoff can get higher lift force for the system.

Acknowledgement: This work is supported by National Natural Science Foundation of China (Project No. 11972261; 11572229), Fundamental Research Funds for the Central Universities (Project No. 22120180063).

Conflicts of Interest: The authors declare that they have no conflicts of interest to report regarding the present study.

References

Alexander, D. (1984): Unusual phase relationships between forewings and hindwings in flying dragonflies. *Journal of Experimental Biology*, vol. 109, pp. 379-383.

Alexander, R. M. (2000): Winging their way. *Nature*, vol. 405, pp. 17-18.

Anderson, J. D. J. (1989): *Introduction to Flight*. McGraw-Hill, NY.

Azuma, A.; Azuma, S.; Watanabe, I.; Furuta, T. (1985): Flight mechanics of a dragonfly. *Journal of Experimental Biology*, vol. 116, pp. 79-107.

Azuma, A.; Watanabe, T. (1988): Flight performance of a dragonfly. *Journal of Experimental Biology*, vol. 137, pp. 221-252.

Bao, L. (2007): *The Mechanics of Flexibility Effects of Insect Wing in Flapping* (*Doctoral Thesis)*. Chinese Academy of Science.

Bergou, A. J.; Xu, S.; Wang, Z. J. (2007): Passive wing pitch reversal in insect flight. *Journal of Fluid Mechanics*, vol. 591, pp. 321-337.

Chang, F. V. (1980): Bending of uniformly cantilever rectangular plates. *Applied Mathematics and Mechanics*, vol. 1, no. 3, pp. 371-383.

Chu, F.; Wang, L.; Zhong, Z.; He, J. (2014): Hermite radial basis collocation method for vibration of functionally graded plates with in-plane material inhomogeneity. *Computers and Structures*, vol. 142, pp. 79-89.

Combes, S. A.; Daniel, T. L. (2003): Flexural stiffness in insect wings II. Spatial distribution and dynamic wing bending. *Journal of Experimental Biology*, vol. 206, pp. 2989-2997.

Daniel, T. L.; Combes, S. A. (2002): Flexible wings and fins: bending by inertial or fluid-dynamic forces? *Integrative and Comparative Biology*, vol. 42, no. 5, pp. 1044-1049.

Dardel, M.; Bakhtiari-Nejad, F. (2010): A reduced order of complete aeroelastic model for limit cycle oscillations. *Aerospace Science and Technology*, vol. 14, pp. 95-105.

Dimitriadis, G.; Giannelis, N. F.; Vio, G. A. (2018): A modal frequency-domain generalised force matrix for the unsteady vortex lattice method. *Journal of Fluids and Structures*, vol. 76, pp. 216-228.

Du, G.; Sun, M. (2008): Effects of unsteady deformation of flapping wing on its aerodynamic forces. *Applied Mathematics and Mechanics*, vol. 29, no. 6, pp. 731-743.

Dwivedi, Y. D.; Bhargava, V. (2019): Aerodynamic characterization of bio inspired corrugated wings. *Applied Bionics Biomechanics*, vol. 3, no. 1, pp. 1-10.

Ellington, C. P. (1984a): The aerodynamics of hovering insect flight. I. The quasi-steady analysis. *Philosophical Transactions of the Royal Society of London. B, Biological Sciences*, vol. 305, no. 1122, pp. 1-15.

Ellington, C. P. (1984b): The aerodynamics of hovering insect flight. II. Morphological parameters. *Philosophical Transactions of the Royal Society of London. B, Biological Sciences*, vol. 305, no. 1122, pp. 17-40.

Hedrick, T. L.; Combes, S. A.; Miller, L. A. (2014): Recent developments in the study of insect flight. *Canadian Journal of Zoology*, vol. 93, no. 12, pp. 925-943.

Ho, W. H.; New, T. H.; Matare, E. (2017): Unsteady CFD analysis of an oscillating aerofoil inspired by dragonfly wings. *Proceedings of Topical Problems of Fluid Mechanics*, pp. 150-166.

Hou, D.; Yin, Y.; Zhong, Z.; Zhao, H. (2015): A new torsion control mechnism induced by blood circulation in dragonlfy wings. *Bioinspiration & Biomimetics*, vol. 10, 016020.

Hou, D.; Yin, Y.; Zhong, Z.; Zhao, H. (2015): Effects of blood in veins of dragonfly wing on the vibration characteristics. *Computers in Biology and Medicine*, vol. 58, pp. 14-19.

Lehmann, F. O. (2004): The mechanisms of lift enhancement in insect flight. *Naturwissenschaften*, vol. 91, pp.101-122.

Maybury, W. J.; Lehmann, F. O. (2004): The fluid dynamics of flight control by kinematic phase lag variation between two robotic insect wings. *Journal of Experimental Biology*, vol. 207, pp. 4707-4726.

Norberg, R. A. (1975): Hovering flight of the dragonfly Aeschna juncea L., kinematics and aerodynamics. *Swimming and Flying in Nature.* pp. 763-781, Springer, Boston, MA.

Obata, A.; Shinohara, S.; Akimoto, K.; Suzuki, K.; Seki, M. (2014): Aerodynamic bio-mimetics of gliding dragonflies for ultra-light flying robot. *Robotics*, vol. 3, no. 2, pp. 163-180.

Salami, E.; Ward, T. A.; Montazer, E.; Ghazali, N. N. N. (2019): A review of aerodynamic studies on dragonfly flight. *Proceedings of the Institution of Mechanical Engineers, Part C: Journal of Mechanical Engineering Science*, vol. 233, no. 18, pp. 6519-6537.

Savage, S. B. (1979): The role of vortives and unsteady effects during the hovering flight of dragonflies. *Journal of Experimental Biology*, vol. 83, pp. 59-77.

Shumway, N.; Laurence, S. J. (2019): The impact of deformation on the aerodynamics of flapping dragonfly wings. *American Institute of Aeronautics and Astronautics Scitech 2019 Forum*, pp. 1-18.

Sun, M.; Lan, S. L. (2004): A computational study of the aerodynamic forces and power requirements of dragonfly (Aeschna juncea) hovering. *Journal of Experimental Biology*, vol. 207, pp. 1887-1901.

Takahashi, H.; Sato, K.; Matsumoto, K.; Shimoyama, I. (2014): Measuring differential pressures with multiple MEMS sensorsduring takeoff of an insect-like ornithopter. *Journal of Biomechanical Science and Engineering*, vol. 9, no. 1, pp. 1-10.

Tang, D.; Dowell, E. H.; Hall, K. C. (1999): Limit cycle oscillations of a cantilevered wing in low subsonic flow. *American Institute of Aeronautics and Astronautics Journal*, vol. 37, no. 3, pp. 364-371.

Thomas, A. L.; Taylor, G. K.; Srygley, R. B.; Nudds, R. L.; Bomphrey, R. J. (2004): Dragonfly flight: free-flight and tethered flow visualizations reveal a diverse array of unsteady lift-generating mechanisms, controlled primarily via angle of attack. *Journal of Experimental Biology*, vol. 207, pp. 4299-4323.

Uppu, S. P.; Manisha, D.; Devi, G. D.; Chengalwa, P.; Devi, B. V. (2018): Aerodynamic analysis of a dragonfly. *Journal of Advanced Research in Fluid Mechanics and Thermal Sciences*, vol. 51, no. 1, pp. 31-41.

Usherwood, J. R.; Lehmann, F. O. (2008): Phasing of dragonfly wings can improve aerodynamic efficiency by removing swirl. *Journal of the Royal Society Interface*, vol. 5, pp. 1303-1307.

Wakeling, J. M.; Ellington, C. P. (1997): Dragonfly flight I. Gliding flight and steady-state aerodynamic forces. *Journal of Experimental Biology*, vol. 200, pp. 543-556.

Wang, L.; Zhong, Z. (2014): Dynamics of the dragonfly wings raised by blood circulation. *Acta Mechanica*, vol. 225, pp. 1471-1485.

Wang, L.; Zhong, Z. (2015): Radial basis collocation method for the dynamics of rotating flexible tube conveying fluid. *International Journal of Applied Mechanics*, vol. 7, no. 3, pp. 1550045.

Wang, L.; Zhong, Z. (2018): Complex modal analysis for the time-variant dynamical problem of rotating pipe conveying fluid. *Computer Modeling in Engineering & Sciences*, vol. 114, no. 1, pp. 1-18.

Wang, L. H.; Hu, Z. D.; Zhong, Z.; Ju, J. W. (2009): Hamiltonian dynamic analysis of an axially translating beam featuring time-variant velocity. *Acta Mechanica*, vol. 206, no. 3-4, pp. 149-161.

Wang, L. H.; Hu, Z. D.; Zhong, Z.; Ju, J. W. (2010): Dynamic analysis of an axially translating viscoelastic beam with an arbitrarily varying length. *Acta Mechanica*, vol. 214, no. 3-4, pp. 225-244.

Wang, Z. J. (2004): The role of drag in insect hovering. *Journal of Experimental Biology*, vol. 207, pp. 4147-4155.

Wang, Z. J.; Russell, D. (2007): Effect of forewing and hindwinginteractions on aerodynamic forces and power in hovering dragonfly flight. *Physical Review Letters*, vol. 99, pp. 1-4.

Weis-Fogh, T. (1973): Quick estimates of flight fitness in hovering animals including novel mechanisms for lift production. *Journal of Experimental Biology*, vol. 59, pp. 169-230.

Zhao, H.; Yin, Y.; Zhong, Z. (2010): Micro and nano structures and morphologies on the wing veins of dragonflies. *Chinese Science Bulletin*, vol. 55, no. 19, pp. 1993-1995.

Zhao, H.; Yin, Y.; Zhong, Z. (2013): Arnold circulation and multi-optimal dynamic controlling mechanisms in dragonfly wings. *Acta Mechanica Solida Sinica*, vol. 26, no. 3, pp. 237-244.

Zhu, J.; Zhou, C.; Wang, C.; Jiang, L. (2014): Effect of flexibility on flapping wing characteristics under forward flight. *Fluid Dynamics Research*, vol. 46, pp. 1-18.

Appendix A

The resulting equations for obtaining the coefficients c_j, b_i, r_j, η in Eq. (8) are expressed as follows:

$$(1-\mu)\frac{\pi}{4}\frac{\alpha_j}{\operatorname{sh}\alpha_j}\left[\frac{1+\nu}{1-\nu}+\alpha_j\coth\alpha_j\right]+2\frac{b}{l}\sum_{i=1}\frac{b_i}{i}\frac{\frac{j^2}{i^2}+(2-\nu)\frac{b^2}{l^2}}{\left(\frac{j^2}{i^2}+\frac{b^2}{l^2}\right)^2}$$
$$+\frac{b^2}{4\pi D}\frac{r_j}{j^2}\left[\coth\alpha_j-\frac{\alpha_j}{\operatorname{sh}^2\alpha_j}\right]+\frac{q_0b^4x}{\pi^4Dl}\frac{1}{j^5}\left(\tanh\frac{\alpha_j}{2}-\frac{\frac{\alpha_j}{2}}{\operatorname{ch}^2\frac{\alpha_j}{2}}\right)+\frac{2\eta b}{j^2\pi}=0 \tag{A.1}$$

$$-\frac{q_0b^4x}{D\pi^4l}\frac{2}{j^5}\left[(3-\nu)\tanh\frac{\alpha_j}{2}-(1-\nu)\frac{\frac{\alpha_j}{2}}{\operatorname{ch}^2\frac{\alpha_j}{2}}\right]+4(1-\nu)^2\frac{b^3}{l^3}\sum_{i=1}\frac{b_i}{i}\frac{\cos i\pi}{\left(\frac{j^2}{i^2}+\frac{b^2}{l^2}\right)^2}$$
$$+(1-\nu)^2\pi\frac{c_j}{2}\left[\frac{3+\mu}{1-\mu}\coth\alpha_j+\frac{\alpha_j}{\operatorname{sh}^2\alpha_j}\right]-(1+\nu)\frac{b^2}{2\pi D}\frac{r_j}{j^2\operatorname{sh}\alpha_j}\left[1+\frac{1-\nu}{1+\nu}\alpha_j\coth\alpha_j\right]=0 \tag{A.2}$$

$$-\frac{q_0 L^4 x}{D\pi^4 l}\frac{1}{i^5}\left[(3-\nu)\tanh\frac{\beta_i}{2}-(1-\nu)\frac{\frac{\beta_i}{2}}{\mathrm{ch}^2\frac{\beta_i}{2}}\right]-(1-\nu)^2\frac{l^3}{b^3}\cos i\pi\sum_{j=1,3\ldots}\frac{c_j}{j\left(\frac{L^2}{b^2}+\frac{i^2}{j^2}\right)^2}$$

$$+\frac{1}{i^2\pi^2}\frac{l^3}{Db}\sum_{j=1,3\ldots}\frac{r_j\left[\frac{l^2}{b^2}+(2-\nu)\frac{i^2}{j^2}\right]}{j\left(\frac{l^2}{b^2}+\frac{i^2}{j^2}\right)^2}+\frac{\pi}{4}(1-\nu)^2 b_i\frac{\mathrm{ch}\,\beta_i-1}{\mathrm{sh}\,\beta_i}\left[\frac{3+\nu}{1-\nu}-\frac{\beta_i}{\mathrm{sh}\,\beta_i}\right]=0 \tag{A.3}$$

$$\frac{b^2}{l^2}\sum_{i=1}b_i i^2\cos i\pi\left[\frac{\mathrm{ch}\,\beta_i-1}{\mathrm{sh}\,\beta_i}\left(\beta_i\coth\beta_i+\frac{1+\nu}{1-\nu}\right)-\beta_i\right]-$$

$$\frac{1}{(1-\nu)\pi^2}\frac{b^2}{D}\sum_{j=1,3\ldots}\frac{r_j}{\mathrm{sh}\,\alpha_j}(\alpha_j\coth\alpha_j-1)+\sum_{j=1,3\ldots}m^2 c_j\cos j\pi\left[\frac{1+\nu}{1-\nu}\coth\alpha_j+\frac{\alpha_j}{\mathrm{sh}^2\alpha_j}\right] \tag{A.4}$$

$$+\frac{4}{(1-\nu)\pi}\frac{q_0 b^4 x}{D\pi^4 l}\sum_{j=1,3\ldots}\frac{1}{j^3}\left(\tanh\frac{\alpha_j}{2}-\frac{\frac{\alpha_j}{2}}{\mathrm{ch}^2\frac{\alpha_j}{2}}\right)=0$$